Performance Evaluation of SensL SiPM Arrays for High-Resolution PET

Jonathan D. Thiessen, Carl Jackson, Kevin O'Neill, Daryl Bishop, Piotr Kozlowski, Fabrice Retière, Ehsan Shams, Greg Stortz, Christopher J. Thompson, and Andrew L. Goertzen

***Abstract*— Silicon photomultipliers (SiPMs) have high gain, excellent timing performance, and are well suited to PET/MRI applications due, in part, to their MR-compatibility and small form factor. Within the constraints of a resistor-based multiplexing circuit, it is useful to evaluate the four generations of SiPM arrays manufactured by SensL: the SPMArray4, ArraySL-4, ArraySM-4, and ArraySB-4. Breakdown voltage and dark current were measured as a function of temperature in two each of the four generations of SensL SiPM arrays. Flood histograms were created with a ^{68}Ge-irradiated 9x9 LYSO crystal array at temperatures of 5 °C to 45 °C in 5 °C increments and overvoltages of 2 to 4 V in 0.5 V increments. Measurements of dark current vs. bias voltage increased as temperature increased, with a corresponding increase in the breakdown voltage, V_b. The temperature dependence of V_b is similar between all four generations of SiPM arrays with slopes ranging from 17.0 to 23.8 mV/°C. Notably, the ArraySB-4 has lower values for the breakdown voltage, with V_b = 24 V at 0 °C. Mean energy resolution for individual LYSO crystals showed improvements in each successive generation. The average energy resolution of the ArraySB-4 was 11.9% after correcting for non-linearity in the SiPM pixels. The linearity of the SensL SiPM arrays as a function of temperature and breakdown voltage makes them a suitable choice for a high-resolution, small animal PET/MRI system. Based on its improved resolvability and energy resolution, lower sensitivity to temperature and higher PDE, the ArraySB-4 will be used in our PET system.**

***Keywords*— PET, silicon photomultiplier, small animal PET, hybrid PET/MRI**

Manuscript received November 22, 2013.

This work was supported by the Natural Sciences Engineering Research Council of Canada through Discovery Grants 341628 to A.L. Goertzen and 36672 to C.J. Thompson, University of Manitoba Amalgamated Research Fund, and through a Manitoba Health Research Council and Terry Fox Research Institute Postdoctoral Fellowship to J.D. Thiessen. ArraySM-4 and ArraySB-4 SiPM arrays provided by SensL.

J.D Thiessen is with the Department of Radiology, University of Manitoba, Winnipeg, Manitoba, Canada. Phone +1 (204) 789-3478, e-mail: Jonathan.Thiessen@med.umanitoba.ca

C. Jackson and K. O'Neill are with SensL, Cork, Ireland.

D. Bishop and F. Retiere are with the Detector Development Group, TRIUMF, Vancouver, British Columbia, Canada.

P. Kozlowski is with the Department of Radiology, University of British Columbia, Vancouver, British Columbia, Canada.

E. Shams is in the Graduate Program of Biomedical Engineering, University of Manitoba, Winnipeg, Manitoba, Canada.

V. Sossi and G. Stortz are with the Department of Physics & Astronomy, University of British Columbia, Vancouver, British Columbia, Canada.

C.J. Thompson is an Emeritus Professor of the Montreal Neurological Institute, McGill University, Montréal, Québec, Canada.

A.L. Goertzen is with the Departments of Radiology and Physics & Astronomy, University of Manitoba, Winnipeg, Manitoba, Canada.

I. Introduction

Our group is developing a high-resolution PET insert that will fit inside and operate simultaneously with a small-animal MRI. Based on Monte Carlo simulations [1] and 3D system response modeling [2], sub-millimeter resolution is anticipated at the center of our current PET insert design.

Towards this goal, an MR-compatible, resistor-based multiplexing transmitter card was developed using a 4x4 SiPM array (SensL, Cork, Ireland), LYSO dual-layer offset crystal array (Proteus Inc., Chagrin Falls, OH), and an HDMI® connection for power supply, temperature monitoring, and analog signal readout [3-5]. Recently, we have evaluated the performance of different SiPM multiplexors [6] and developed a detector interface board and slow control system for controlling detector bias and monitoring temperature and power consumption [7]. Within the constraints of our detector circuit, it is useful to evaluate the four generations of SiPM arrays manufactured by SensL: the SPMArray4, ArraySL-4, ArraySM-4, and ArraySB-4 (labeled as A, L, M, and B) as a function of temperature and bias voltage in a real-world system.

II. Data Acquisition and Temperature Control

A. Detector Module and Interface Board

The detector card multiplexes SiPM signals from 16 to 4 with a charge division resistor network and transmits signals via 4 differential amplifiers (Analog Devices AD8132). Differential signals are read out and bias voltage and ±2.8 V amplifier power are supplied via an 8m-long HDMI® v1.4 Type A to Type C cable (BrightLink Cables). Differential signals are received with 4 differential receivers (Analog Devices AD8130) and output as negative-going, 50Ω single-ended signals via SMA connectors along with a fast sum signal for triggering. Since the current detector interface board and slow control system can only supply and monitor positive bias voltages [7] and the ArraySB-4 requires a negative bias voltage, bias voltage was supplied and monitored using a programmable power supply (Agilent N6700B with a 100V/0.5A N6736B DC power module) and bias current monitored with a digital multimeter (Agilent 34410A) – both controlled using a custom LabWindows™/CVI application.

B. Temperature Control

The detector card was placed in a light-tight plastic enclosure (Budde Industries) insulated with 0.5" polystyrene insulation painted flat black (Rust-Oleum). Temperature was controlled using an air-to-air thermoelectric assembly (Laird Technologies AA-034-12-22) and PID temperature controller (Laird Technologies PR-59) with ±0.05°C control stability.

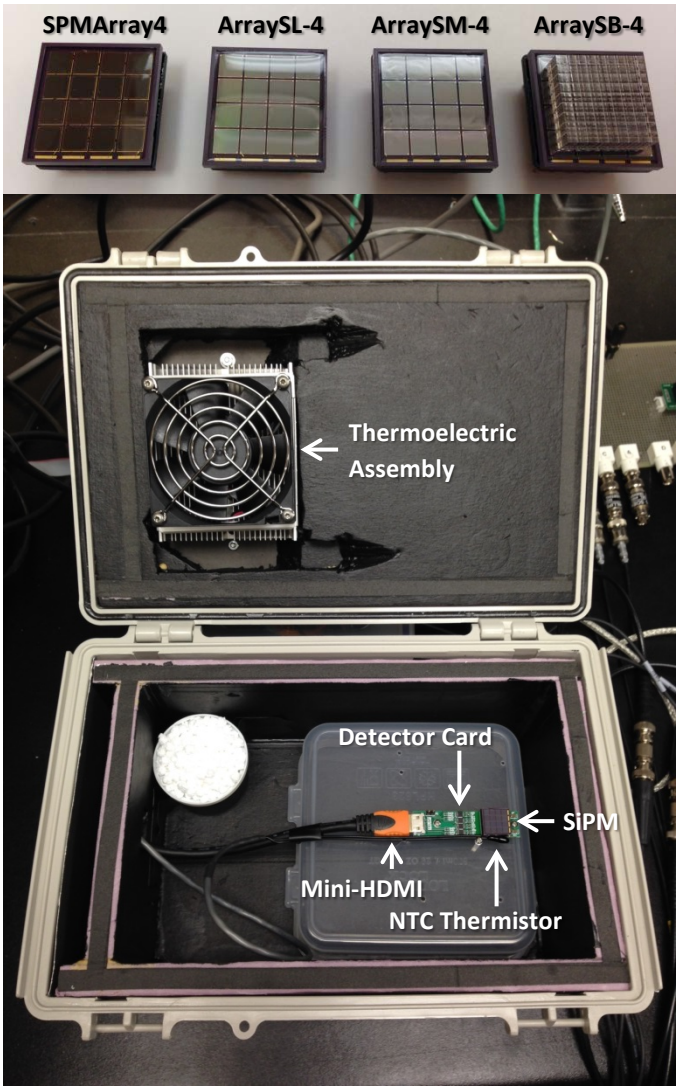

Fig. 1. Top: Four generations of the SensL SiPM array. Bottom: Temperature control chamber with HDMI-connected detector card and NTC thermistor.

Temperature was monitored with a ±0.05°C precision NTC thermistor attached to the side of the SiPM array (Fig. 1).

C. *Temperature- and Bias-Dependent Measurements*

All measurements were conducted with two each of the A-, L-, M-, and B-series SensL arrays (Fig. 1). Output signals were processed using standard NIM electronics and digitized with a PC-based DAQ card (National Instruments PCI-6133) previously described in [8].

At each temperature, dark current was measured at bias voltages ranging from 25-31 V (N-on-P arrays with positive bias: A, L, M) or 22-28 V (P-on-N array with negative bias: B) in 0.1 V increments. In order to determine the breakdown voltage, dark current vs. bias voltage was fit to:

$$I(V) = K\frac{(V-V_b)^2}{1-N_{ca}(V-V_b)^2} \quad (1)$$

where V_b is the breakdown voltage, K is a scaling factor encompassing the temperature dependent dark noise rate, and $N_{ca}(V - V_b)^2$ is the mean correlated avalanches per avalanche [9].

A 9x9 LYSO array with a 1.2x1.2x3.5 mm^3 crystal pitch (Proteus Inc.) was directly coupled to the SiPM arrays with optical grease. All crystal surfaces were polished and a bonded enhanced specular reflector (ESR) was used as the reflector between crystals. ESR was also optically coupled to the top of the LYSO array and the sides and top were wrapped in several layers of white Teflon tape. Detector flood histogram data and energy spectra were acquired by flood irradiating the detector with a ^{68}Ge source, acquiring 250,000 counts at each temperature and bias voltage. Energy resolutions and photopeak amplitudes were calculated for each crystal element at 5 overvoltages above V_b (2, 2.5, 3, 3.5, and 4 V) and 9 temperatures (5°C to 45°C in 5°C increments). Images of flood histograms were generated using a 250-750 keV energy window based on the mean photopeak amplitude of all 81 crystals. Image scale was set as the min/max value in each flood histogram. All data were analyzed in Matlab.

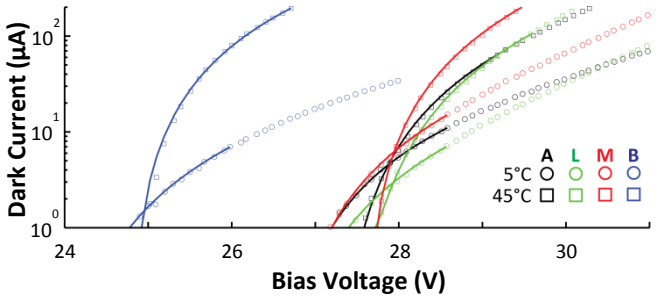

Fig. 2. Dark current vs. bias voltage with fit (solid line) for A-, L-, M-, and B-series SiPM arrays at 5 °C and 45 °C.

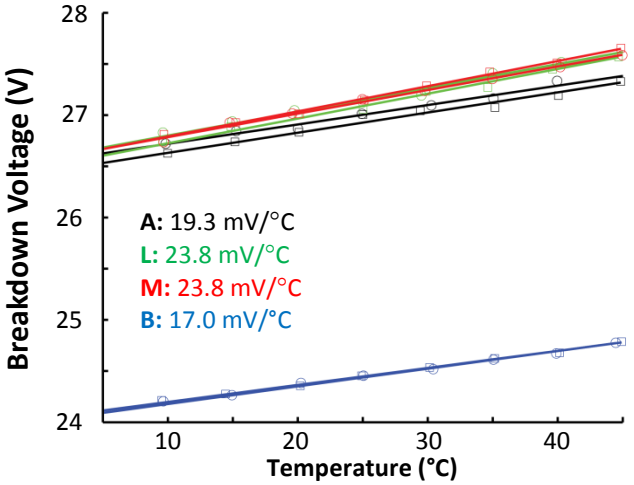

Fig. 3. Breakdown voltage vs. temperature shows a linear relationship for all four generations. The ArraySB-4 has the lowest breakdown voltage and smallest temperature dependence.

III. Results and Discussion

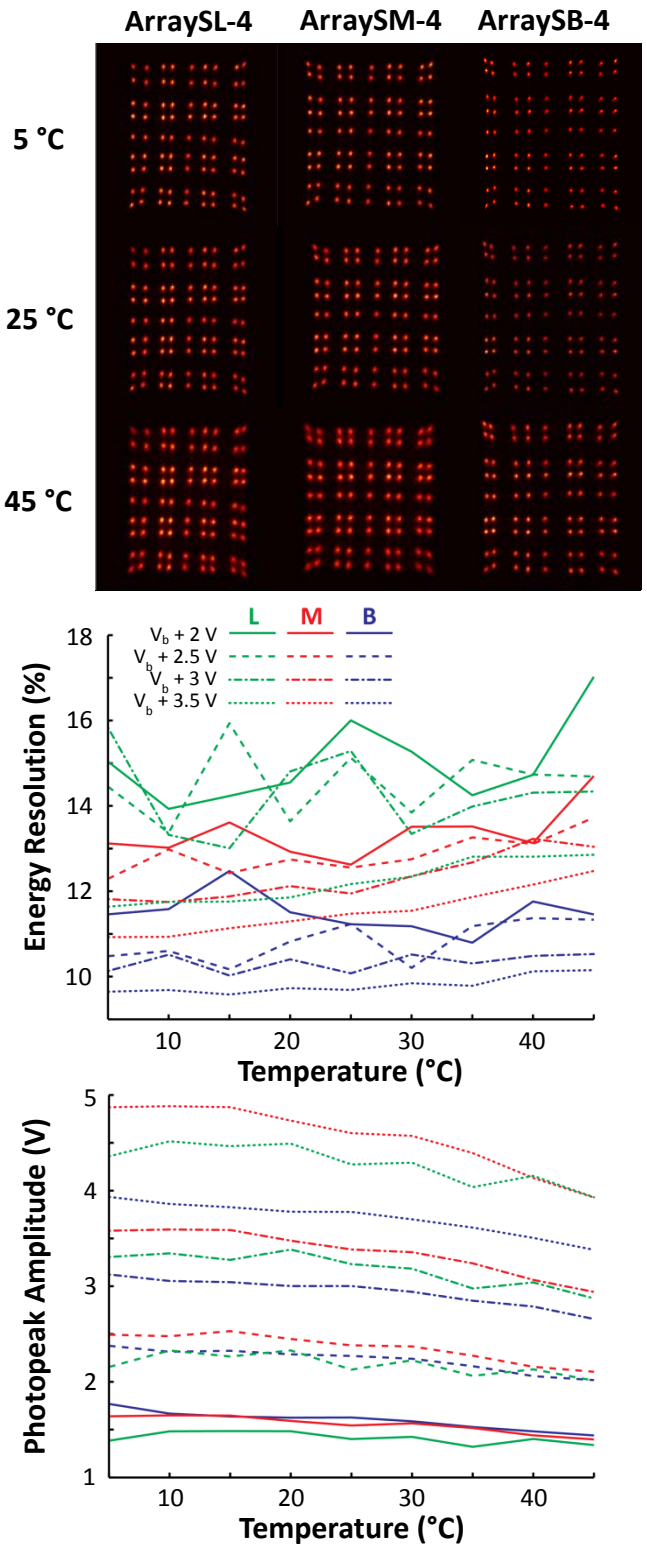

Fig. 4. Flood histograms (top), energy resolution (middle) and photopeak amplitude (bottom) as a function of temperature. Resolvability and energy resolution improves with each successive SiPM generation as a function of temperature. Photopeak amplitude is relatively linear as a function of temperature when at a constant overvoltage above the temperature-dependent breakdown voltage.

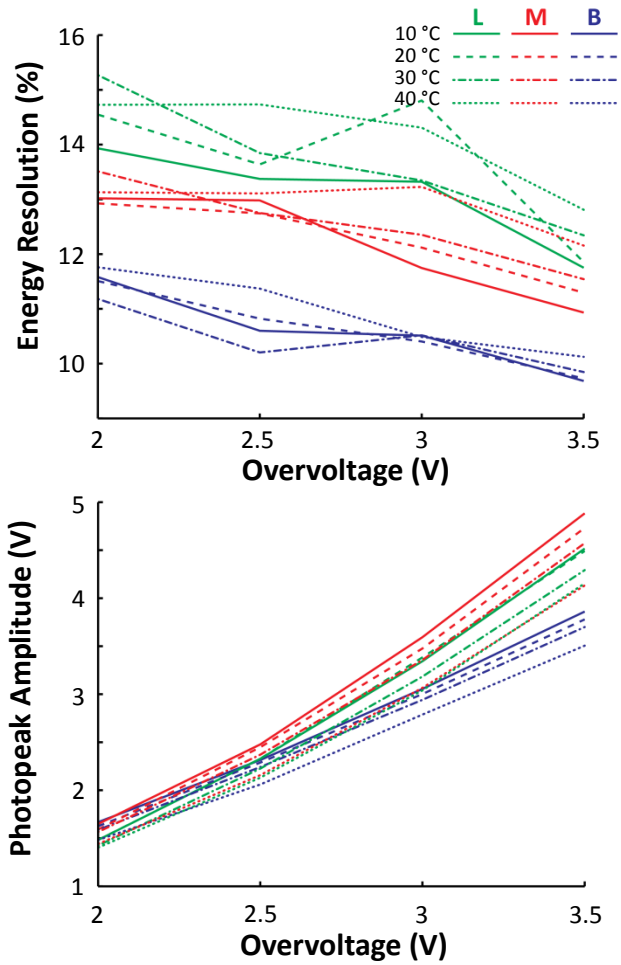

Fig. 5. Energy resolution (top) and photopeak amplitude (bottom) as a function of overvoltage. Energy resolution improves as overvoltage increases. Photopeak amplitude increases relatively linearly as overvoltage increases.

A. Breakdown Voltage vs. Temperature

Figure 2 shows the dark current vs. bias voltage for A-, L-, M-, and B-series SiPM arrays at 5 °C and 45 °C. Dark current increases as a function of both bias voltage and temperature. Based on a fit to Eq. 1, the breakdown voltage increases linearly as a function of temperature (Fig. 3), with the slope varying from 17.0 mV/°C for the ArraySB-4 to 23.8 mV/°C for the ArraySL-4 and ArraySM-4. The ArraySB-4 has a lower breakdown voltage and decreased temperature dependence.

B. Flood and Energy Histograms

Figure 4 shows the flood histograms from the ArraySL-4, ArraySM-4, and ArraySB-4 at an overvoltage of 3 V and temperatures of 5, 25, and 45 °C. All crystals were well resolved. Based on visual inspection, the ArraySB-4 has better resolvability at different temperatures and overvoltages.

Energy resolution improves with each successive SiPM generation (L, M, and B) as a function of temperature (Fig. 4) and overvoltage (Fig. 5), likely due to improvements in photon detection efficiency (PDE) and signal gain. When measuring energy resolution vs. temperature at lower overvoltages, variability in the fitting routine and noise in the data prevent

any clear trend from being distinguished (Fig. 4). However, at Vb + 3.5 V (dotted lines), increased gain allows us to distinguish a slight improvement in energy resolution as temperature decreases. It is easier to see improvements in energy resolution as the overvoltage increases, also due to increased PDE and gain of the SiPM arrays (Fig. 5). Photopeak amplitude is relatively linear as a function of temperature and overvoltage, suggesting our method for determining breakdown voltage can be used to accurately set signal gain. Decreasing photopeak amplitude vs. temperature can be attributed to lower LYSO light output as temperature increases [10].

C. Energy Correction for Non-Linearity

In the previous section, energy resolution was calculated assuming a linear relationship between photopeak amplitude and gamma ray energy. In order to account for non-linearity in the SiPM pixels and LYSO light output, photopeaks were measured for 4 sources with different gamma energies: ^{57}Co (122 keV), ^{133}Ba (356 keV), ^{68}Ge (511 keV), and ^{137}Cs (662 keV) at 25°C and V_b + 3V. A calibration curve was determined for each crystal based on a 2nd order polynomial fit and corrected energy histograms were generated. Corrected energy histograms had slightly increased energy resolutions, from 1.3% (B-series) to 2.2% (M-series), suggesting there is a small compression of the 511 keV signal (Table 1). The relatively low saturation effects can be attributed, in part, to the light-sharing properties of the crystal array and optical coupling.

TABLE I.
CORRECTED ENERGY RESOLUTION AND PHOTOPEAK AMPLITUDE

SiPM Array	Energy Resolution		Photopeak Amplitude	
	Original	*Corrected*	*Original (V)*	*Corrected (keV)*
L	13.3 ± 1.3%	15.1 ± 1.6%	3.2 ± 0.4	512 ± 11
M	12.2 ± 0.9%	14.4 ± 1.4%	3.4 ± 0.3	513 ± 5
B	10.6 ± 1.0%	11.9 ± 1.4%	2.7 ± 0.3	511 ± 7

IV. CONCLUSION

Based on its improved resolvability and energy resolution, lower sensitivity to temperature and higher PDE, the ArraySB-4 will be used in our high-resolution PET/MRI system.

REFERENCES

[1] G. Stortz, M. D. Walker, C. J. Thompson, A. L. Goertzen, F. Retière, X. Zhang, J. D. Thiessen, P. Kozlowski, and V. Sossi, "Characterization of a New MR Compatible Small Animal PET Scanner Using Monte-Carlo Simulations," *IEEE Trans. Nucl. Sci.*, vol. 60, no. 3, pp. 1637–1644, Jun. 2013.

[2] X. Zhang, G. Stortz, V. Sossi, C. J. Thompson, F. Retière, P. Kozlowski, J. D. Thiessen, and A. L. Goertzen, "Development and evaluation of a LOR-based image reconstruction with 3D system response modeling for a PET insert with dual-layer offset crystal design," *Phys. Med. Biol.*, vol. 58, no. 23, pp 8379–8399, Nov. 2013.

[3] A. L. Goertzen, X. Zhang, M. M. McClarty, E. J. Berg, C.-Y. Liu, P. Kozlowski, F. Retière, L. Ryner, V. Sossi, G. Stortz, and C. J. Thompson, "Design and Performance of a Resistor Multiplexing Readout Circuit for a SiPM Detector," *IEEE Trans. Nucl. Sci.*, vol. 60, no. 3, pp. 1541–1549, Jun. 2013.

[4] A. L. Goertzen, J. D. Thiessen, X. Zhang, C.-Y. Liu, E. Berg, D. Bishop, P. Kozlowski, F. Retière, V. Sossi, G. Stortz, and C. J. Thompson, "Application of HDMI® cables as an MRI compatible single cable solution for Readout and power supply of SiPM based PET detectors," in *2012 IEEE Nuclear Science Symposium and Medical Imaging Conference Record (NSS/MIC)*, 2012, pp. 3184–3188.

[5] C. J. Thompson, A. L. Goertzen, E. J. Berg, F. Retière, P. Kozlowski, L. Ryner, G. Stortz, and V. Sossi, "Evaluation of High Density Pixellated Crystal Blocks With SiPM Readout as Candidates for PET/MR Detectors in a Small Animal PET Insert," *IEEE Trans. Nucl. Sci.*, vol. 59, no. 5, pp. 1791–1797, Oct. 2012.

[6] C. J. Thompson, A. L. Goertzen, J. D. Thiessen, D. Bishop, F. Retière, P. Kozlowski, G. Stortz, and V. Sossi. "Measurement of Energy and Timing Resolution of Very Highly Pixellated LYSO Crystal Blocks with Multiplexed SiPM Readout for Use in a Small Animal PET/MR Insert," in *2013 IEEE NSS/MIC*, 2013, M12-41.

[7] E. Shams, J. D. Thiessen, D. Bishop, P. Kozlowski, F. Retière, V. Sossi, G. Stortz, C. J. Thompsons, and A. L. Goertzen, "A PET Detector Interface Board and Slow Control System Based on the Raspberry Pi®," in *2013 IEEE NSS/MIC*, 2013, M16-42.

[8] B. McIntosh, D. B. Stout, and A. L. Goertzen, "Validation of a GATE Model of ^{176}Lu Intrinsic Radioactivity in LSO PET Systems," *IEEE Trans. Nucl. Sci.*, vol. 58, no. 3, pp 682-686, Jun. 2011.

[9] A. Vacheret *et al.*, "Characterization and simulation of the response of Multi-Pixel Photon Counters to low light levels," *Nucl. Instrum. Meth. A*, vol. 656, 2011, pp 69-83.

[10] S. Weber, D. Christ, M. Kurzeja, R. Engels, G. Kemmerling, and H. Halling, "Comparison of LuYAP, LSO, and BGO as Scintillators for High Resolution PET Detectors," *IEEE Trans. Nucl. Sci.*, vol. 50, no. 5, 2003, pp 1370-1372.

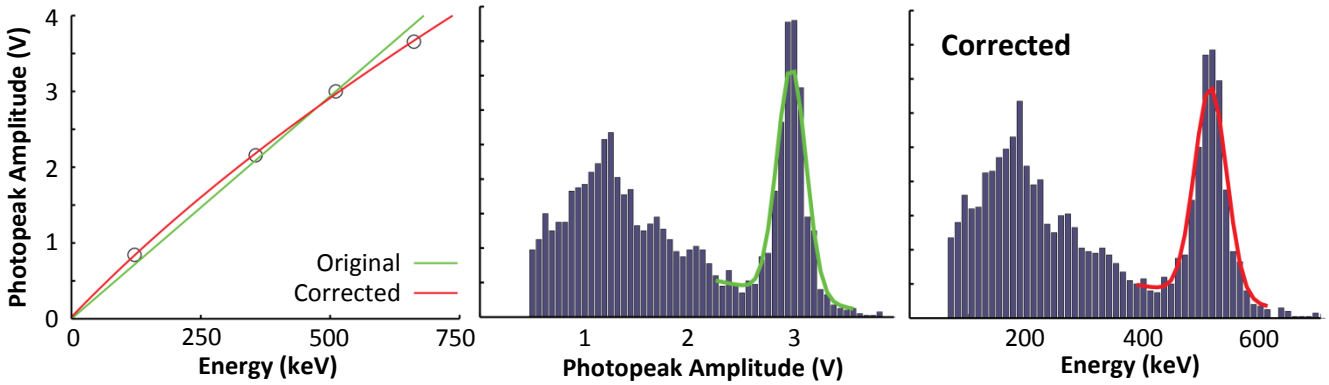

Fig. 6. Left: Photopeak amplitude vs. gamma ray energy for a single crystal with linear fit through 0 and 511 keV (green) and 2nd order polynomial fit through all 4 sources (red). Original (middle) and corrected (right) energy histograms with fitted Gaussian curves.